Piezo-to-Piezo (P2P) Conversion: Simultaneous β-Phase Crystallization and Poling of Ultrathin, Transparent and Freestanding Homopolymer PVDF Films via MHz-Order Nanoelectromechanical Vibration

Robert Komljenovic,[†] Peter C. Sherrell,[‡] Eirini Goudeli,[¶] Amgad R. Rezk,[*,†] and Leslie Y. Yeo[†]

[†]*Micro/Nanophysics Research Laboratory, School of Engineering, RMIT University, Melbourne, VIC 3001, Australia*

[‡]*Applied Chemistry and Environmental Science, School of Science, RMIT University, Melbourne, VIC 3001, Australia*

[¶]*Laboratory of Aerosol Particle Technology, Department of Chemical Engineering, The University of Melbourne, Parkville, VIC 3052, Australia*

E-mail: amgad.rezk@rmit.edu.au

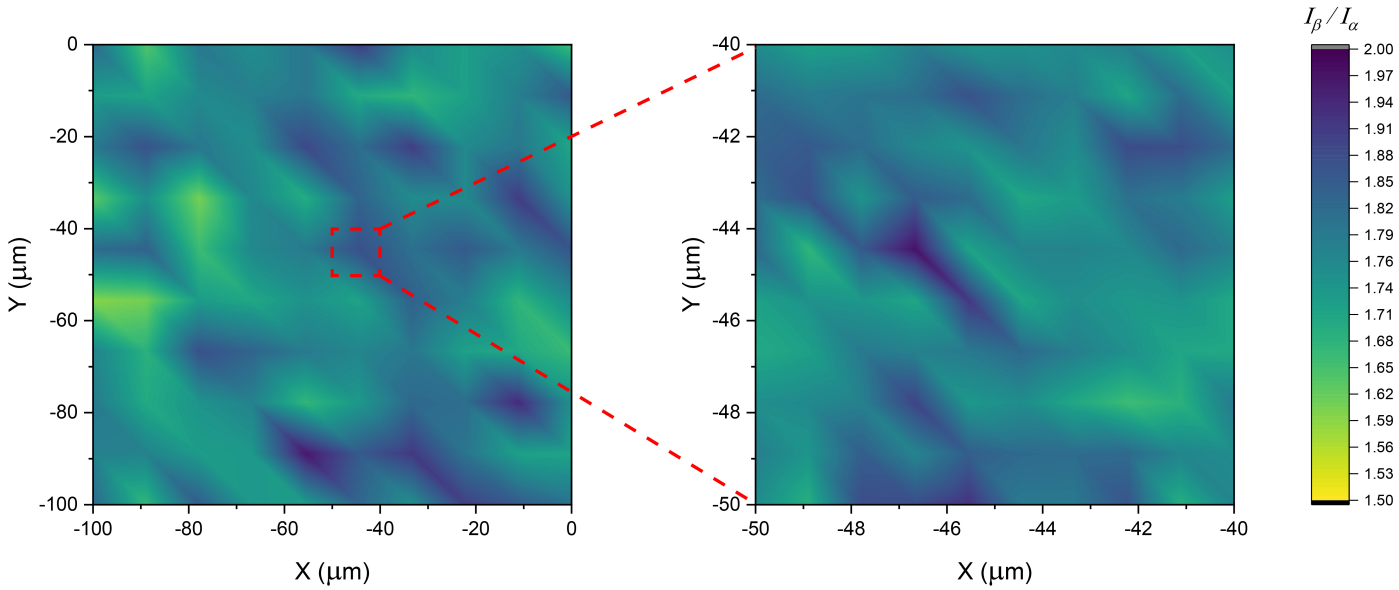

Figure 1: Confocal Raman microscopy map of a 100 μm ×100 μm area on the surface of a EM-SRBW PVDF film, showing local distributions of the α- and β-phases, quantified by the relative intensity between the Raman β-phase peak at 839 cm^{-1} and the α-phase peak at 794 cm^{-1} (I_β/I_α). The magnified inset represents an area of 10 μm × 10 μm.

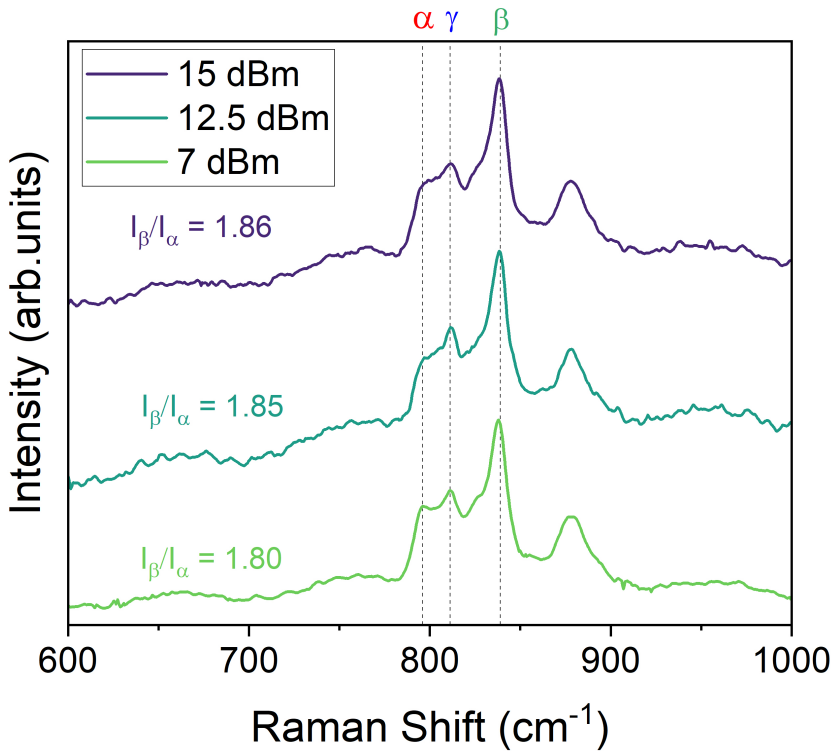

Figure 2: Variation in the phase composition of EM-SRBW PVDF films synthesized at different input SRBW powers, as quantified using Raman spectroscopy.

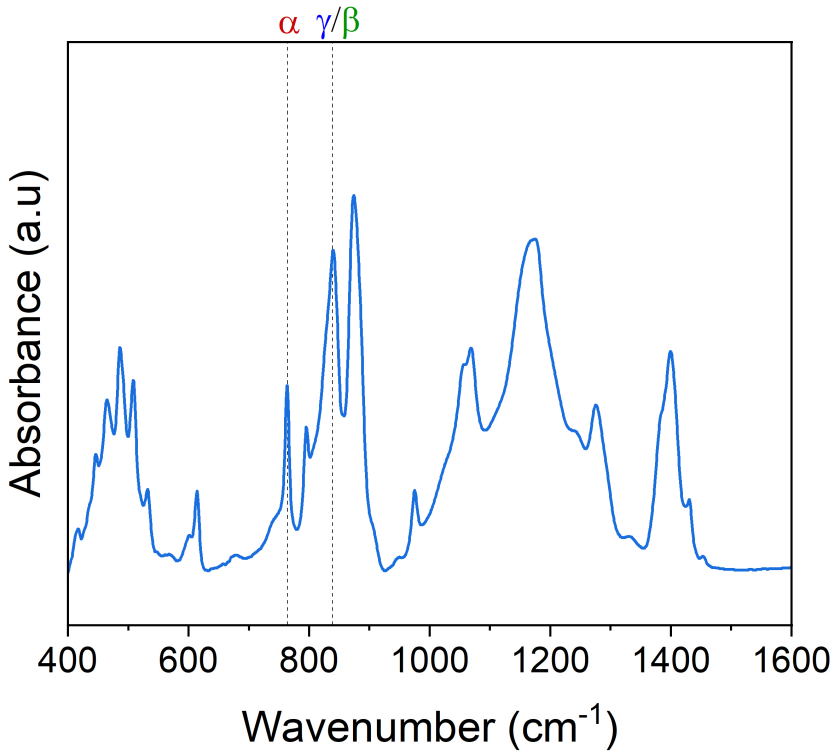

Figure 3: Fourier Transform infrared (FTIR) spectra for the 6 μm commercially-poled PVDF film. The FTIR peaks for the α- and β-phases are located at 763 and 841 cm^{-1}, respectively.

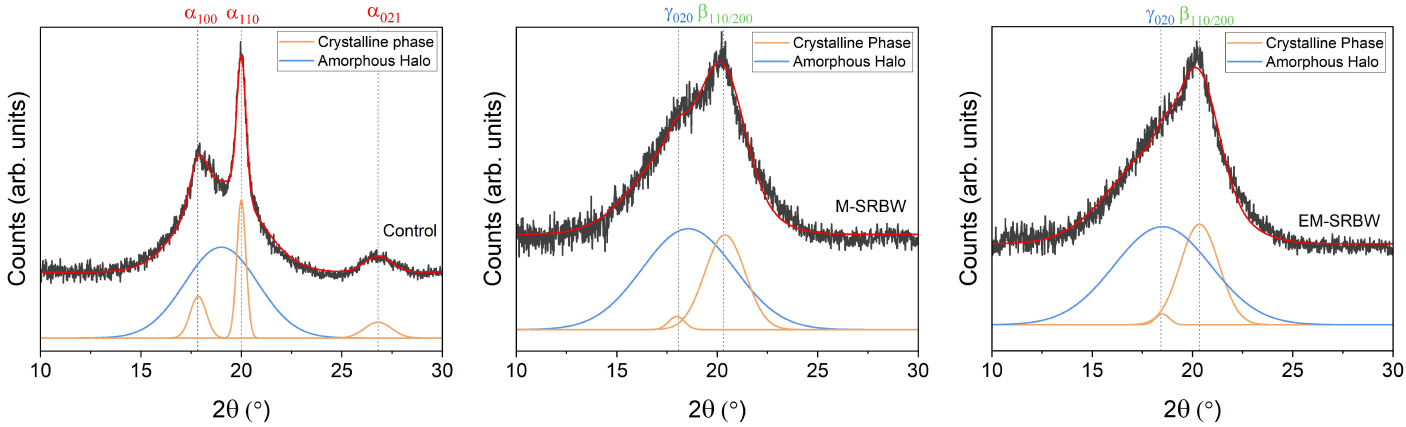

Figure 4: Deconvoluted XRD profiles showing fitting of the original data with the relevant crystalline diffraction peaks as well as the amorphous halo for the (a) control, (b) M-SRBW, and, (c) EM-SRBW samples. The overall crystallinity obtained via XRD profile deconvolution analysis for the control, M-SRBW, and EM-SRBW films yielded values of 26.3%, 30.2%, and 30.0%, respectively, which is in good qualitative agreement with the trends observed in the differential scanning calorimetry (DSC) data. It is nevertheless well documented that DSC typically has higher sensitivity compared to the XRD (see, for example, Szewczyk et al., *ACS Appl. Mater. Interfaces* 12, 13575-13583, 2020.)

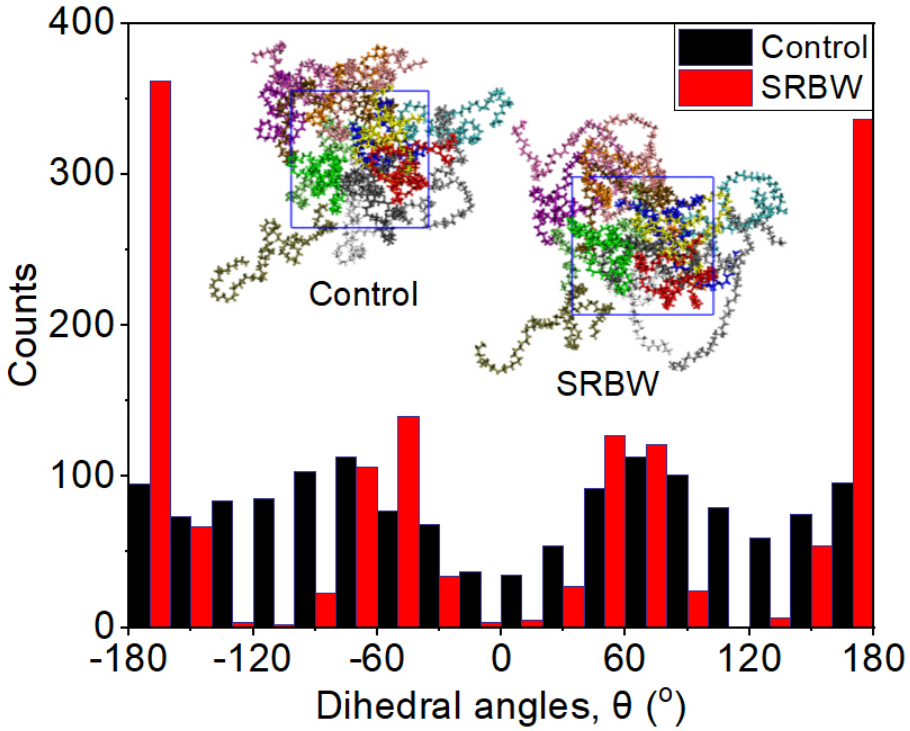

Figure 5: Dihedral angle distribution showing randomly distributed PVDF chains (control; no strain) and that under 1% mechanical strain (due to the SRBW) favoring significant alignment to the trans confirmation (near $-180°$ and $180°$).

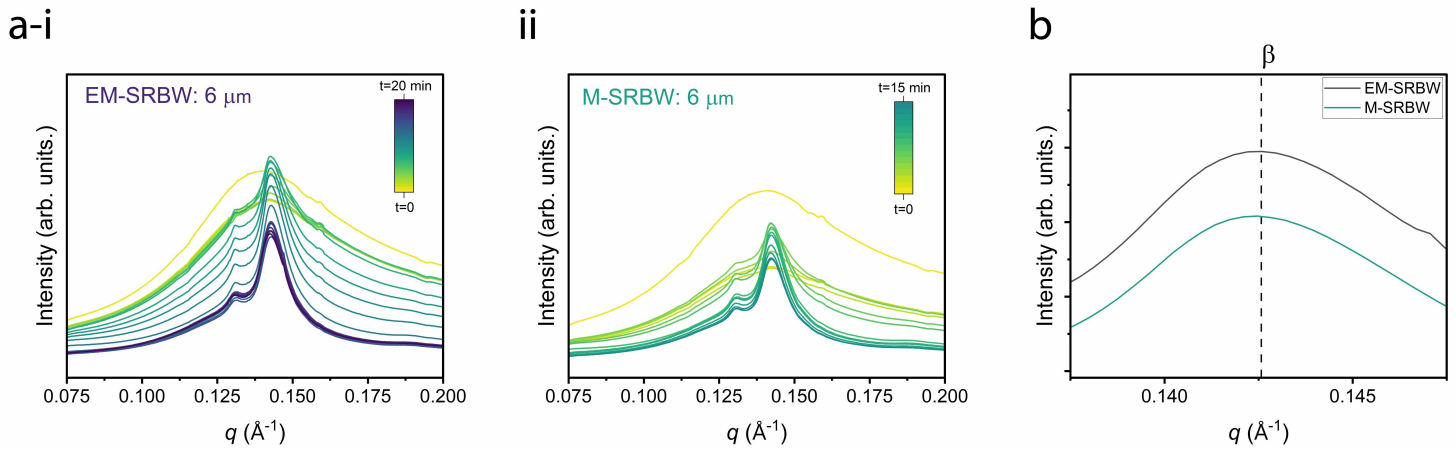

Figure 6: (a) *In situ* GIWAXS measurements of the PVDF films under the (i) EM-SRBW and (ii) M-SRBW forcing (identical data to that shown in Fig. S13) for a given film thickness (6 μm). (b) Plot showing the steady-state spectra, indicating no noticeable shift in the resultant phase.

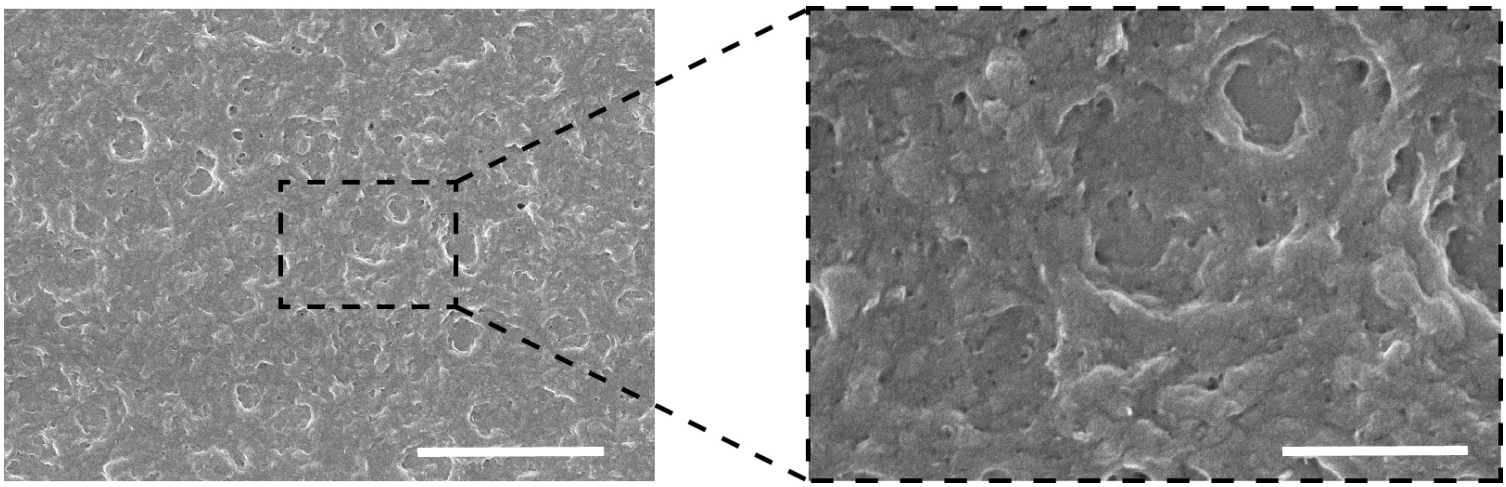

Figure 7: Scanning electron microscopy (SEM) image showing the surface of the post-wet-etched PVDF film (scale bars: 4 μm (left image) and 800 nm (right image)).

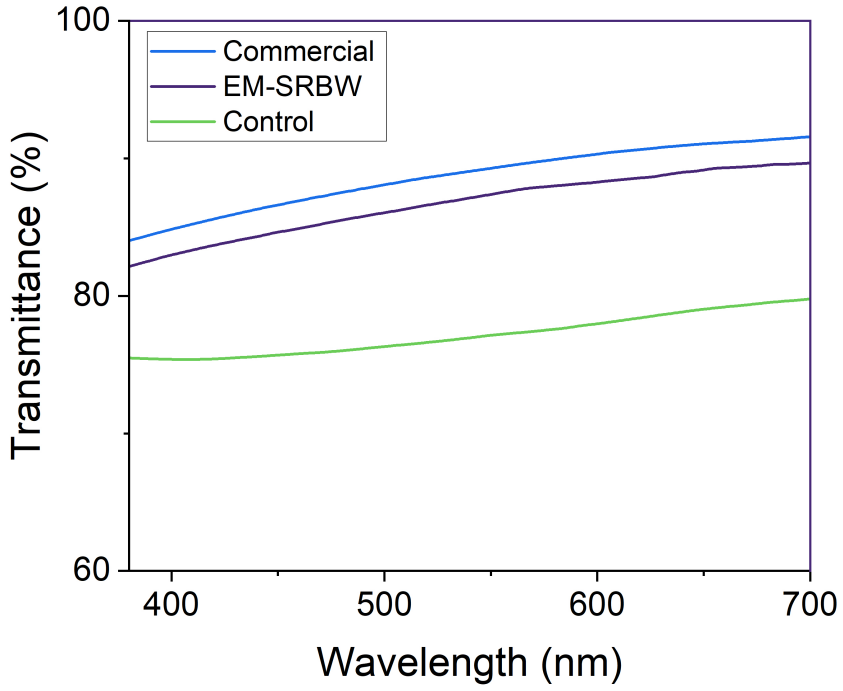

Figure 8: Total light transmittance of the control, commercially-poled and EM-SRBW PVDF films (6 µm thick) showing a transparency at 650 nm of 89%, 91% and 79% for the EM-SRBW, commercial and control films, respectively.

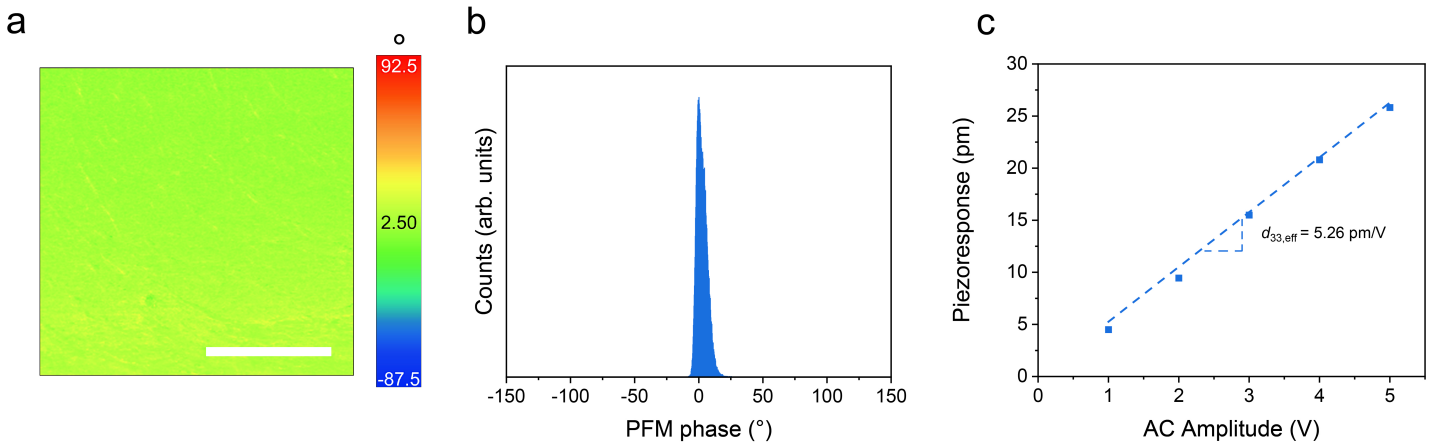

Figure 9: Local polarization of 6 µm thick commercially-poled PVDF films: piezoresponse force microscopy (PFM) (a) phase image, and, (b) phase histogram. (c) Piezoelectric response and corresponding piezoelectric coefficient $d_{33,\text{eff}}$. The scale bars in (a) denote lengths of 2 µm.

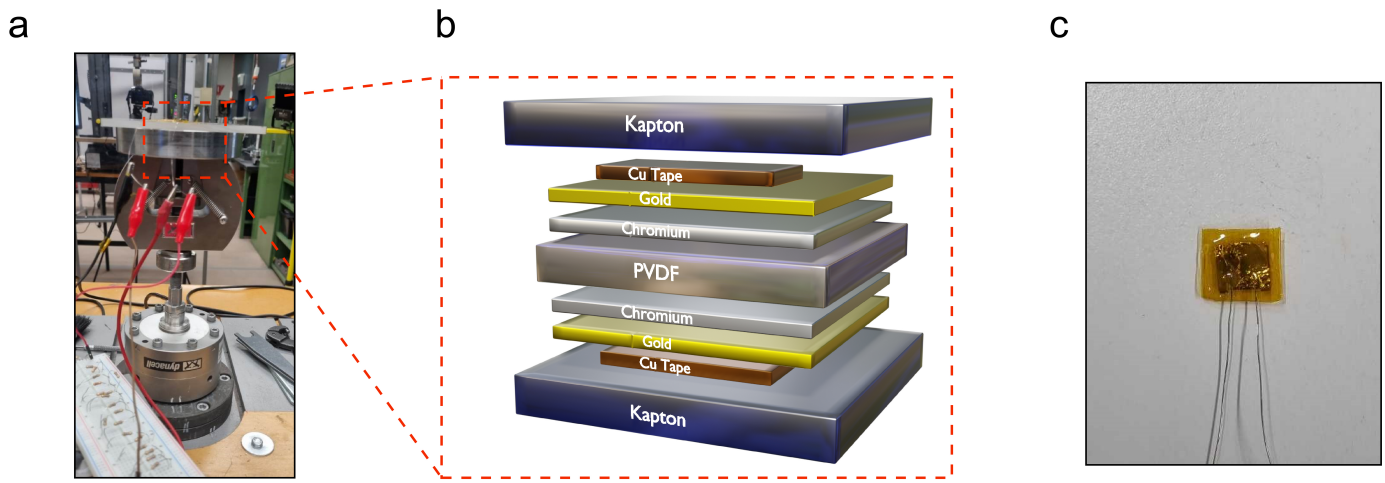

Figure 10: (a) Setup for the macroscopic piezoelectric response measurements of the various piezoelectric energy harvesting (PENG) devices using a dynamic testing instrument (Electropuls E3000; Instron, Norwood, MA, USA). (b) Schematic of the component layout for the PENG devices. (c) Image of an example PENG device.

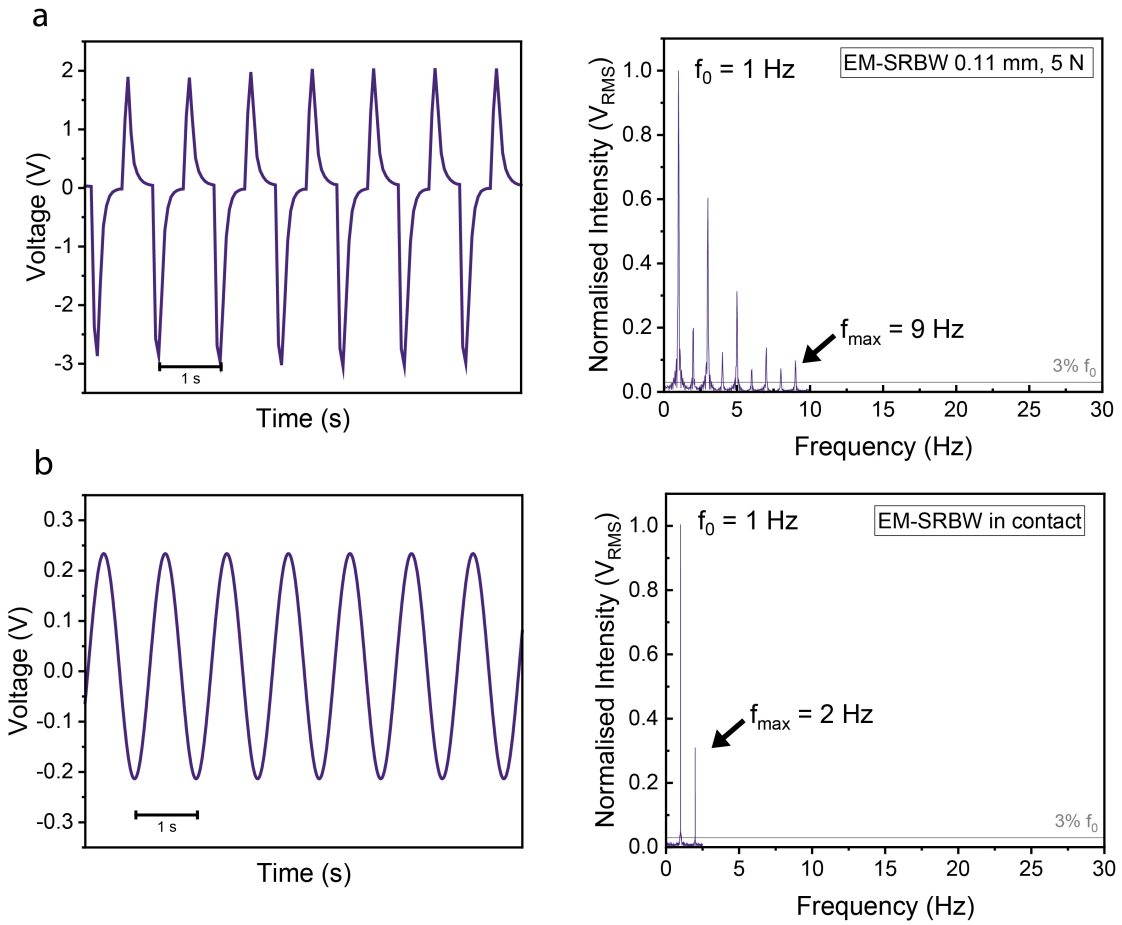

Figure 11: (a) Time domain waveforms and corresponding fast Fourier Transform (FFT) spectrum of signals from macroscopic piezoelectric response measurements with 0.11 mm contact separation, and, (b) under in-contact mode, for the EM-SRBW PENG device.

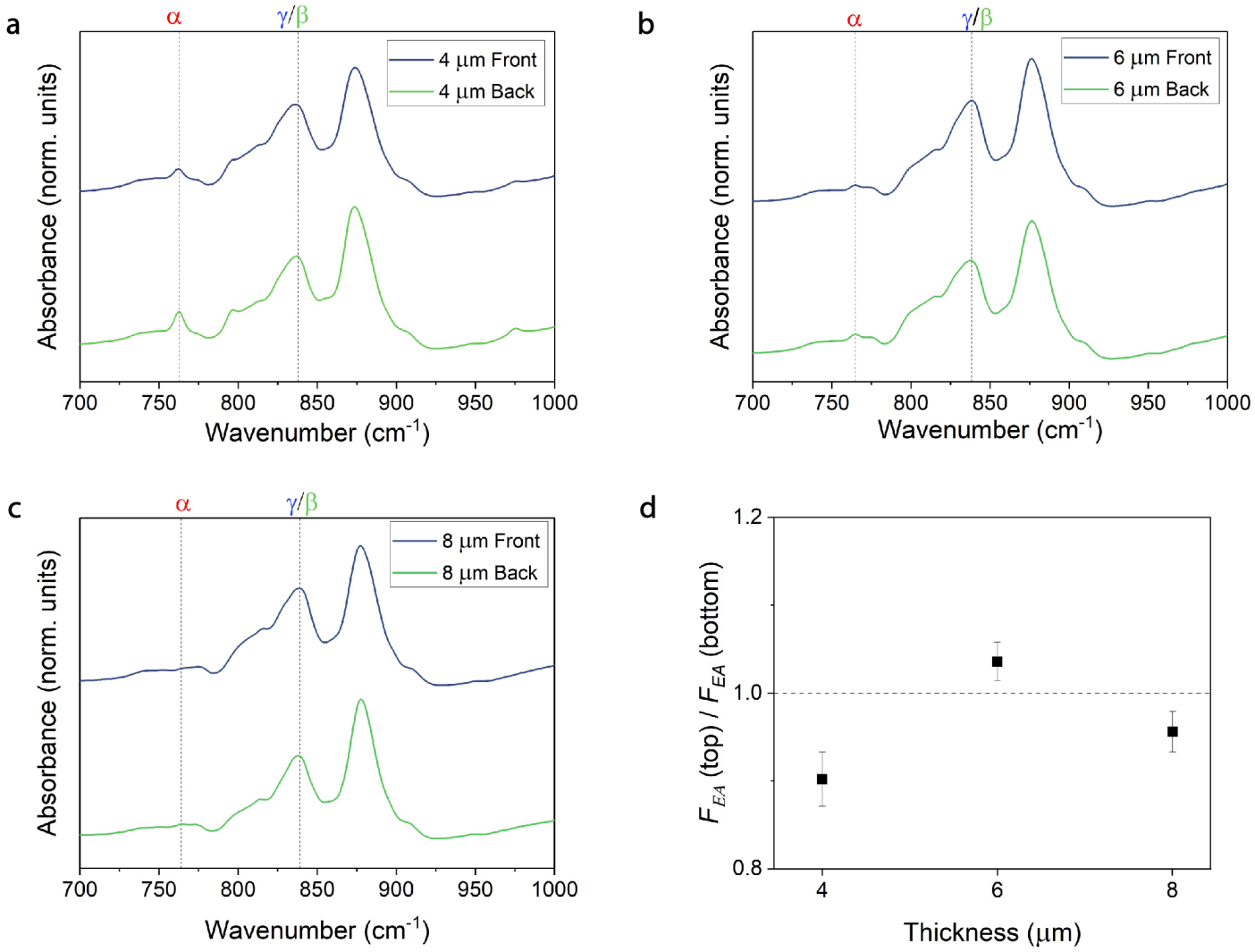

Figure 12: FTIR spectra for (a) 4 (*b*) 6 and (c) 8 μm thick EM-SRBW films. (d) Relative ratio of the electroactive phase content between the top and bottom surfaces of the EM-SRBW films.

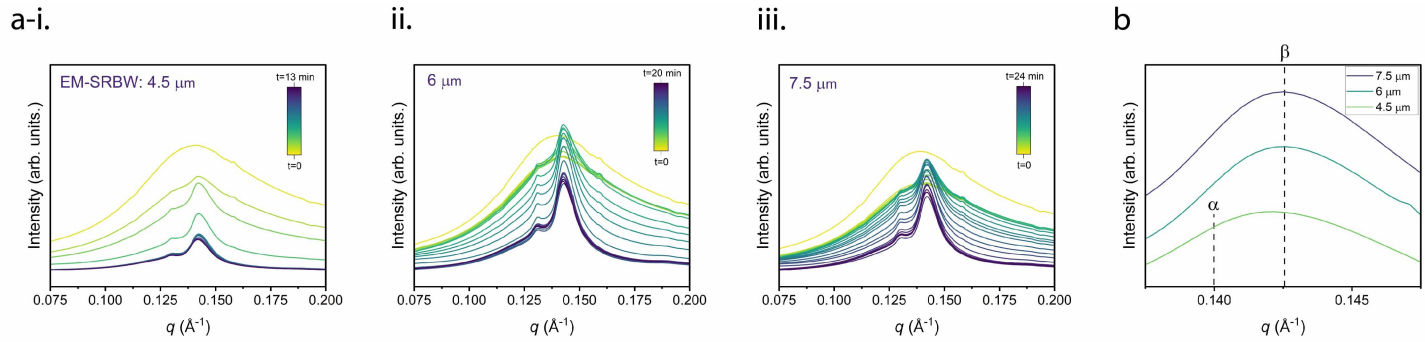

Figure 13: (a) *In situ* GIWAXS measurements of EM-SRBW PVDF films, with varying thicknesses: (i) 4.5 μm, (ii) 6 μm, and, (iii) 7.5 μm. (b) Steady-state spectra in which we note a small shift towards the orthorhombic β-phase, away from the α-phase, for film thicknesses $\geq$ 6 μm.

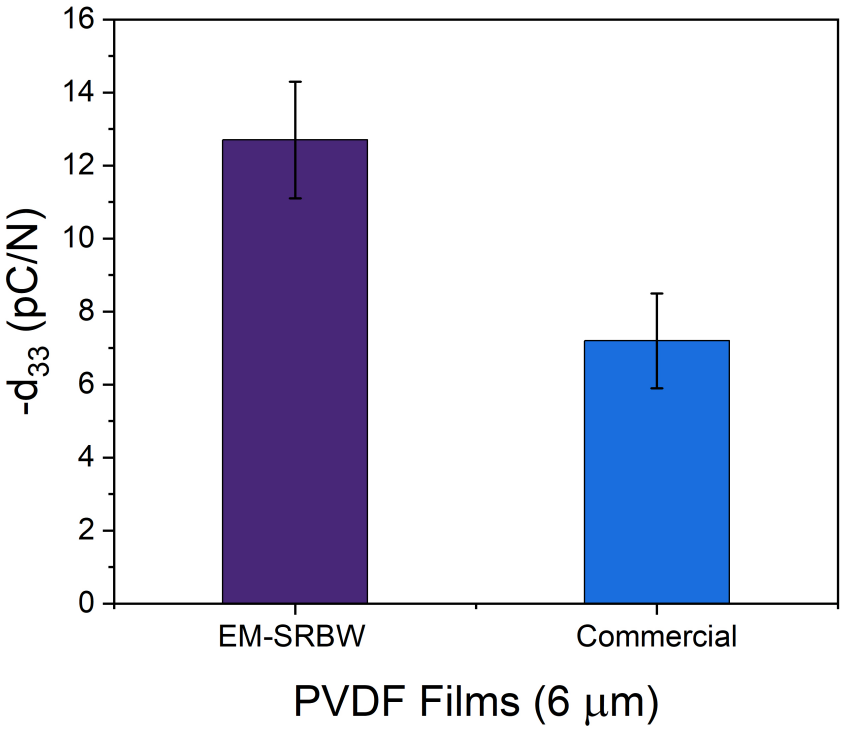

Figure 14: Measurement of the piezoelectric charge coefficient d_{33} for the 6 μm thick EM-SRBW and commercially-poled films using a piezoelectric meter (PKD3-2000; PolyK Technologies LLC, State College, PA, USA) with a 2 N static load.

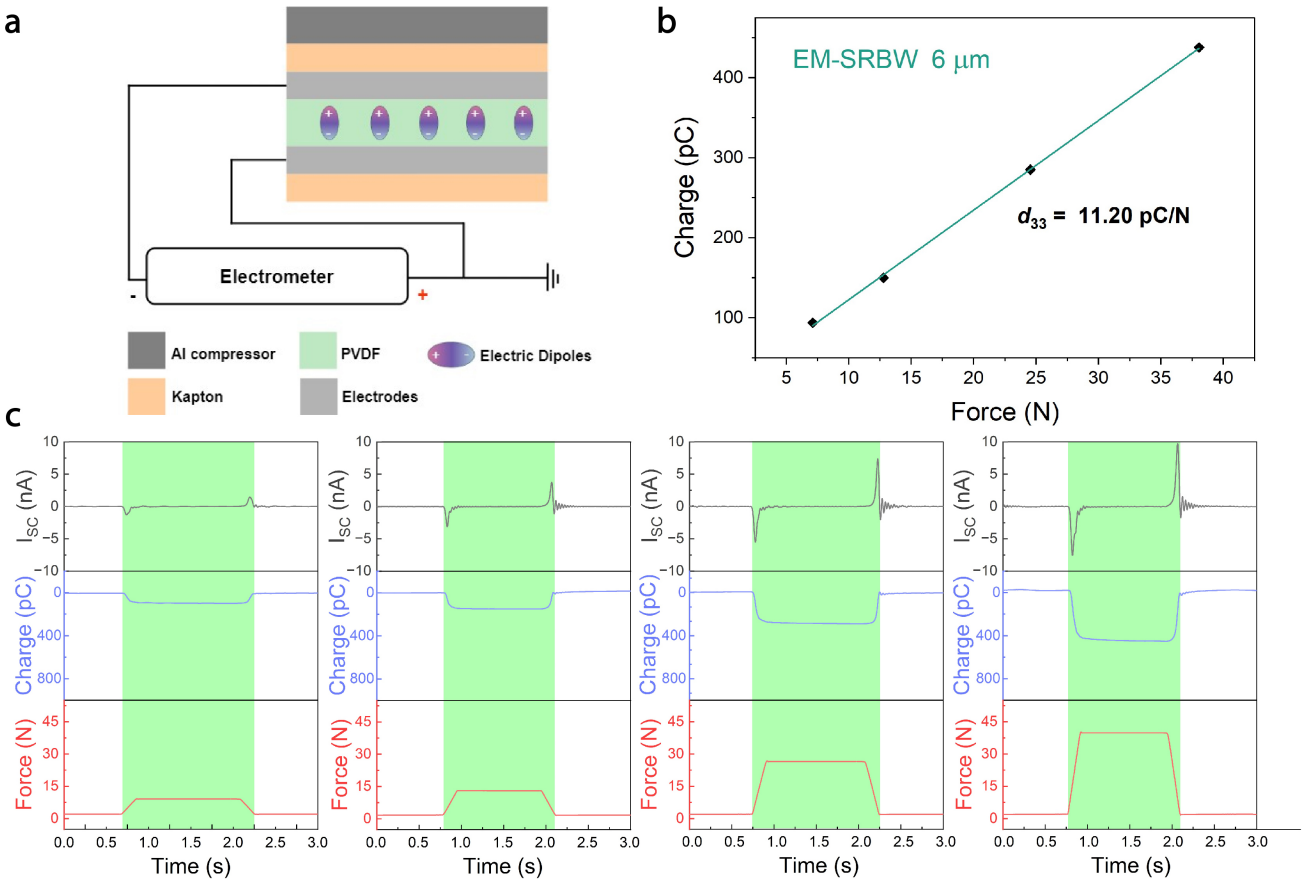

Figure 15: (a) Schematic showing the setup for measuring the piezoelectric output in the negative polarization direction of the PVDF film. (b) Charge–force curve used to calculate the d_{33} value for the EM-SRBW (6 μm) film, obtained from (c) exclusive piezoelectric signals (I_{SC} and charge) through in-contact (2 N preload) measurements at 7.1, 12.7, 24.5 and 38.1 N (left to right panels, respectively); these singular piezoelectric signals occur during the compression and release stages (shaded green area).

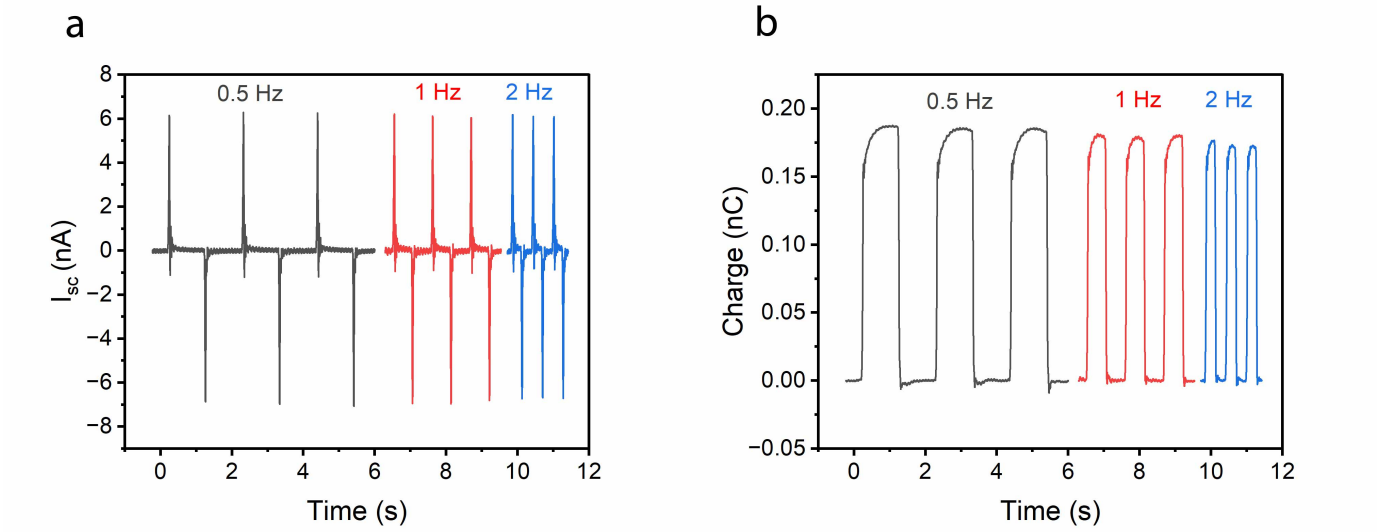

Figure 16: Effect of varying the input frequency on (a) the short circuit current I_{SC}, and, (b) the charge output. All measurements were conducted at a dynamic force of 13 N (2 N–15 N).

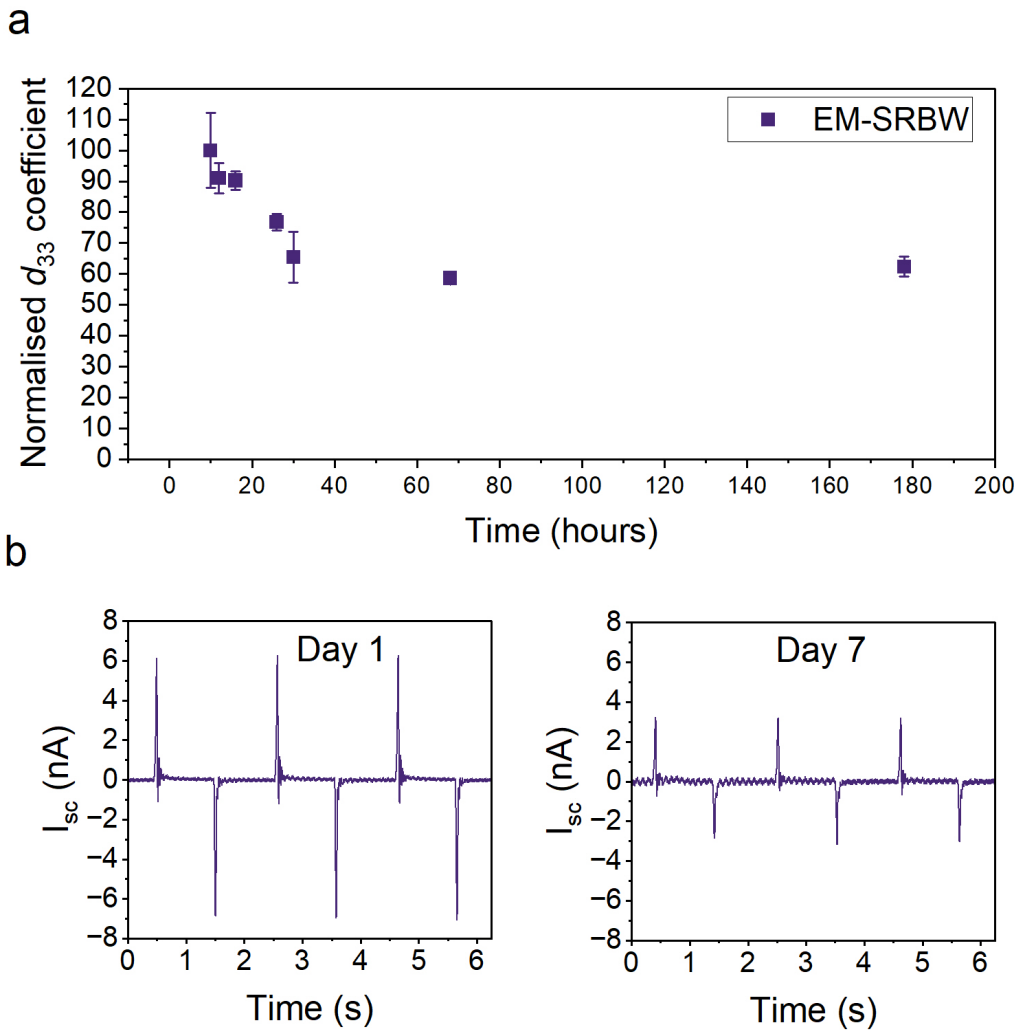

Figure 17: (a) Normalized piezoelectric charge coefficient d_{33} of the EM-SRBW PVDF films up to 7 days of storage under ambient conditions. (b) Representative short-circuit current I_{SC} through in-contact (2 N preload) measurements at 15 N. All error bars indicate ± SD. The short-circuit current data was used to calculate the d_{33} value.

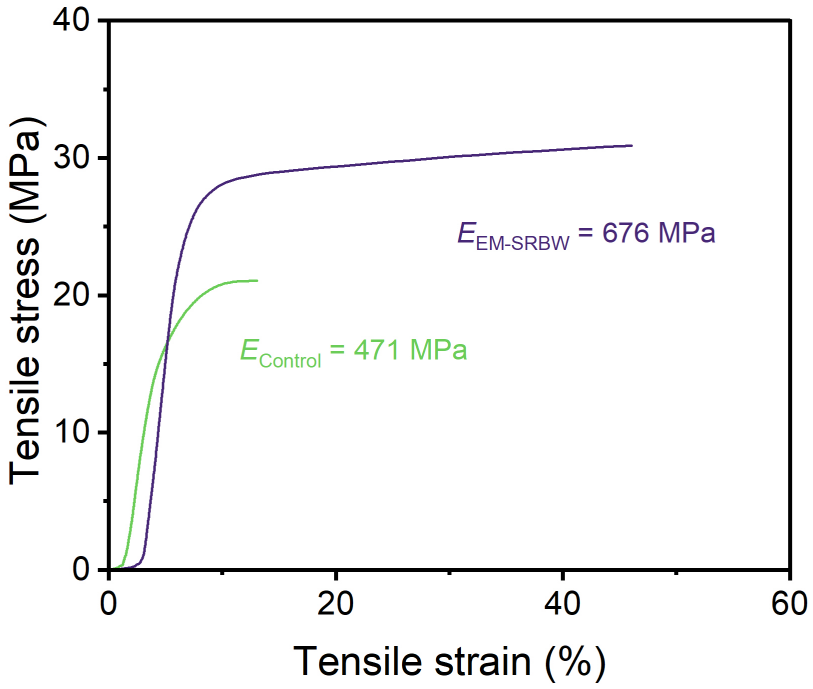

Figure 18: Stress–strain curves of the control and EM-SRBW PVDF films, exhibiting the higher elastic modulus of the EM-SRBW PVDF film ($E = 676$ MPa) compared to that of the control ($E = 471$ MPa).

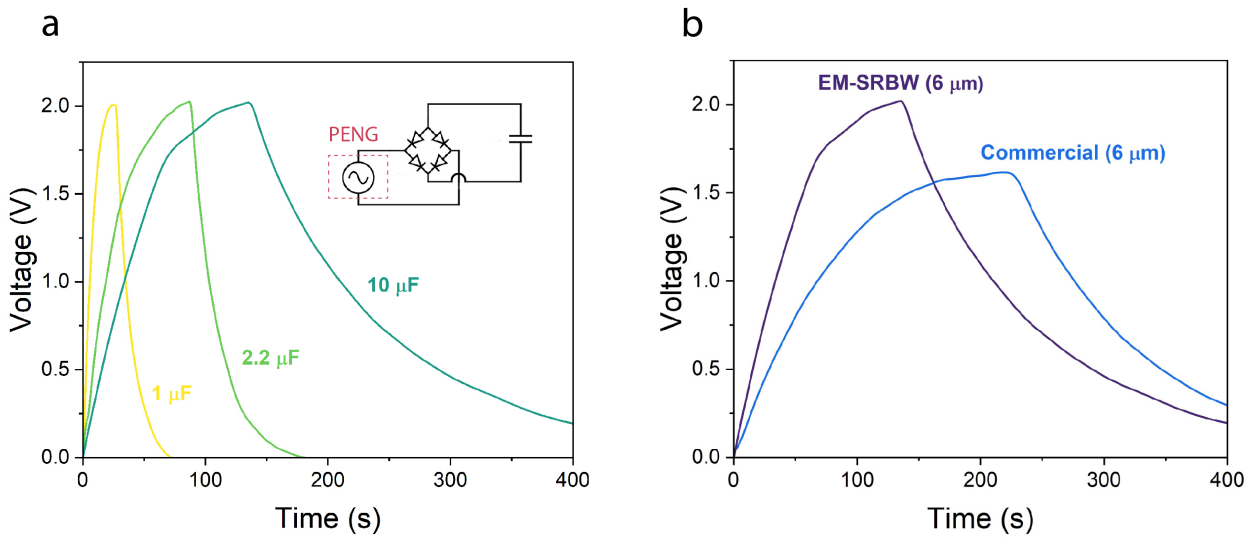

Figure 19: Charge–discharge profiles for PENG devices comprising 6 μm thick EM-SRBW PVDF films when one capacitor (1, 2.2 and 10 μF) was used, and, (b) 6 μm thick EM-SRBW and commercially-poled films when a 10 μF capacitor was utilized. The insert in (a) shows the variable capacitor being charged from voltages supplied by the PENG through the use of a bridge rectifier.